HSPA5 repressed ferroptosis to promote colorectal cancer development by maintaining GPX4 stability

Ronglin WANG#, Lei HUA#, Peixiang MA#, Yang SONG, Jie MIN, Yongdong GUO, Cheng YANG, Junqiang LI*, Haichuan SU*

Department of Oncology, Tangdu Hospital, Air Force Medical University, Xi'an, Shaanxi, China

Correspondence: suhc@fmmu.edu.cn; jjunqiang@126.com
#Contributed equally to this work.

Colorectal cancer (CRC) is one of the most malignant cancers and its pathological mechanism is largely unknown. Unfolded protein response and ferroptosis are both critical factors involved in CRC development. However, their relationship in CRC remains to be explored. In this study, erastin was used to induce ferroptosis in CRC cells. Ferroptosis was confirmed by the detection of glutathione, malondialdehyde, and lipid reactive oxygen species. The CRC datasets were analyzed using the R software, GEPIA2, and TIMER2.0. The results indicated that GPX4 was decreased when treated with the ferroptosis inducer erastin. As an intrinsic protective pathway, the unfolded protein response was activated and HSPA5 was increased during ferroptosis. HSPA5 was found to attenuate erastin-induced GPX4 decrease, repress ferroptosis, and promote CRC cell growth both in vitro and in vivo. Mechanistically, HSPA5 bound directly to GPX4 and the interaction between HSPA5 and GPX4 increased when treated with erastin for a short time period. Although the HSPA5-GPX4 interaction failed to completely reverse erastin-induced GPX4 decrease, HSPA5 slowed down the GPX4 degradation process and gave CRC cells more time to adjust to erastin toxicity. Additionally, HSPA5 was demonstrated to play a diagnostic role and correlated to the immune microenvironment in CRC patients. Our study demonstrates that increased HSPA5 was an intrinsic protective strategy to resist ferroptosis. Specifically, HSPA5 restrained ferroptosis to promote colorectal cancer development by maintaining GPX4 stability. Our study provides potential diagnostic and therapeutic targets for patients with CRC.

Key words: colorectal cancer, unfolded protein response, HSPA5, ferroptosis, GPX4

Colorectal cancer (CRC) is one of the most malignant cancers worldwide. Many patients develop metastases when they are first diagnosed. Surgical resection, chemotherapy, and immunotherapy have been used to treat CRC despite their poor prognosis [1]. Obesity, alcohol consumption, and lack of physical activity have been reported to be related to the pathogenesis of CRC [2]. However, the specific molecular mechanisms of the disease are unclear. Therefore, research efforts are urgently needed to unravel the mechanism and provide novel therapeutic targets for CRC diagnosis and treatment.

Ferroptosis was first defined as regulated cell death in 2012 [3]. The excessive accumulation of iron in the cytoplasm yields a substantial production of peroxide, which induces the oxidation of polyunsaturated fatty acids and subsequent rupture of the cell membrane [4]. The primary anti-oxidation mechanism is mediated by glutathione peroxidase 4 (GPX4). Post glutathione consumption, GPX4 converts lipid hydro-

peroxides to lipid alcohols to prevent iron-mediated toxicity [5]. GPX4 has been reported to promote the development of multiple cancers [6, 7], and the effects of GPX4 were explored and validated. Some studies have recently focused on exploring the regulatory mechanism of GPX4. Some microRNAs have been reported to modulate GPX4 expression and ferroptosis [8, 9]. However, the regulatory mechanism of GPX4 is largely unknown and remains to be fully explored.

Unfolded protein response (UPR) is mediated by three primary sensors, PRKR-like ER kinase (PERK, EIF2AK3), inositol-requiring enzyme 1 (IRE1), and activating transcription factor 6 (ATF6). UPR primarily affects protein folding and stability when confronted with environmental or cellular stimuli [10]. HSPA5 is one of the key effectors which is increased in UPR. It maintains the stability of the target proteins by binding to them. Moreover, HSPA5 has been reported to promote cell survival and cancer development

[11]. In pancreatic cancer and glioma, HSPA5 regulates ferroptosis by modulating GPX4 stability [12, 13]. In CRC, HSPA5 has been shown to regulate cell viability and chemotherapy resistance [13, 14]. However, the effect of HSPA5 on ferroptosis in CRC remains unknown. Thus, additional research is required to understand the role of HSPA5 in ferroptosis and CRC development.

In this study, erastin was used to induce ferroptosis in CRC cells. Glutathione (GSH), lipid reactive oxygen species (ROS), and malondialdehyde (MDA) were detected to examine ferroptosis and the UPR sensors and effectors were evaluated. HSPA5 was knocked down to investigate its critical role in ferroptosis. Our results suggest that HSPA5 attenuates ferroptosis and promotes CRC development both *in vitro* and *in vivo*. It was found that HSPA5 mechanically interacts with and maintains GPX4 stability. This study provides potential diagnostic and therapeutic targets for CRC.

Patients and methods

Patient specimens. CRC tissues and corresponding paired normal tissues were obtained from CRC patients who underwent surgical resection at the Tangdu Hospital affiliated with Air Force Medical University (Xi'an, China). The tissues were frozen and stored in liquid nitrogen after resection. All procedures were approved by the Research Ethics Committee of Tangdu Hospital and written informed consent was obtained from all the patients.

Reagents and antibodies. Erastin (S724202), Ferrostatin-1 (S7243), necrosulfonamide (S8251), Z-VAD-FMK (S7023), and chloroquine diphosphate (S4157) were purchased from Selleck (Houston, TX, USA). The CCK-8 assay kit (C008-4) was purchased from 7 Sea (Shanghai, China). FITC Annexin V Apoptosis Detection Kit I (556547) was purchased from BD Biosciences (San Diego, CA, USA). BODIPY™ 581/591 C11 (D3861) was purchased from Thermo Fisher Scientific (Waltham, MA, USA). The MDA detection kit (S0131M) and the GSH/GSSG detection kit (S0053) were purchased from Beyotime (Shanghai, China). Primary antibodies, including anti-p-eIF2α (3398), were purchased from Cell Signaling Technology (Danvers, MA, USA). Anti-p-IRE1 (AP1146), ATF4 (A0201), and GPX4 (A1933) were purchased from Abclonal (Wuhan, China). Anti-CHOP (15204-1-AP), GAPDH (60004-1-Ig), Ki67 (27309-1-AP), HSPA5 (11587-1-AP), and beta-actin (66009-1-Ig) were purchased from Proteintech (Wuhan, China).

Cell lines and cell culture. DLD1 and SW480 CRC cell lines were acquired from Procell Life Science & Technology Company (Wuhan, China). DLD1 cells and SW480 cells were cultured in RPMI 1640 medium (A1049101, Gibco, New York State, USA) and L15 medium (11415064, Gibco, New York State, USA), respectively. The media were supplemented with 10% fetal bovine serum (26010074, Gibco, New York State, USA) and 1% penicillin-streptomycin. The cell lines were incubated at 37°C with 5% CO$_2$. The HSPA5

stable knockdown cells were constructed by infecting the cells with lentivirus encoding the shRNA targets to HSPA5 (WZ biosciences, Jinan, China). HSPA5-shRNA-1 GTACC-GGAGATTCAGCAACTGGTTAAAGCTCGAGCTT-TAACCAGTTGCTGAATCTTTTTG); HSPA5-shRNA-2 CCGGGAAATCGAAAGGATGGTTAATCTCGAGATTA-ACCATCCTTTCGATTTCTTTTTG). When the cells were 70% confluent, they were cultured with lentivirus mixed with polybrene (40804ES, Yeasen, China) for 48 h. Then, the cells were treated with 4 µg/ml puromycin to kill uninfected cells. The knockdown effect was examined via western blotting.

Western blot. The cells or tissues were lysed with lysis buffer (P0013C, Beyotime, Shanghai, China) supplemented with a phosphatase inhibitor (04906837001, Roche, Basel, Switzerland) and a protease inhibitor (04693159001, Roche, Basel, Switzerland). The cells were incubated on ice for 30 min. The cells were centrifuged at 12,000×g for 15 min and the supernatant was collected. Protein concentration was determined using a BCA Protein Assay Kit (23225, Thermo, MA, US). Proteins were separated by 10% SDS-PAGE, and the protein bands were transferred to polyvinylidene fluoride membranes. The membranes were blocked with 5% non-fat milk and incubated with the target primary antibodies at 4°C overnight. Then, the membranes were washed with TBST buffer and were incubated with HRP goat anti-rabbit IgG (AS014, Abclonal, China) or HRP goat anti-mouse IgG (AS003, Abclonal, China) for 2 h at 25°C. Protein bands were analyzed using Bio-Rad ChemiDocXRS+ (170-8265, Bio-Rad, California, USA).

Immunoprecipitation. The cells were lysed using a gentle lysis buffer (P0013, Beyotime, Shanghai, China) supplemented with a phosphatase inhibitor and a protease inhibitor. The supernatant was collected as described in the western blot section. 3 µg of primary antibodies anti-GPX4 or anti-HSPA5 were added to the supernatant and incubated at 4°C for 8 h. Protein A/G immunoprecipitation magnetic beads (B23201, Bimake, TX, USA) were added and incubated for another 4 h. The beads were then collected and washed. Finally, the proteins were analyzed as described in the western blot section.

Immunohistochemistry. The harvested mouse tumor tissues were fixed in 4% paraformaldehyde. Tissue sections were deparaffinized using xylene. Different concentrations of ethanol were used to rehydrate these sections. The peroxide activity was repressed using 3% hydrogen peroxide and blocked the sections with 5% normal goat serum for 30 min at room temperature. The sections were then incubated overnight at 4°C with a primary antibody against Ki67 (27309-1-AP, Proteintech, Wuhan, China). Finally, the sections were stained with diaminobenzidine and hematoxylin.

Cell proliferation assay. 1×10^4 DLD1 and SW480 cells were seeded into the wells of a 96-well plate. The cells were incubated in an incubator for 16 h. Pretreated cells with ZVAD-FMK (10 µM), necrosulfonamide (0.5 µM), chloroquine diphosphate (20 µM), or ferrostatin-1 (1 µM) for 2 h

before treatment with indicated concentrations of erastin for 24 h. CCK-8 reagent was added to corresponding media to generate a working solution (1:9). The medium was discarded, and the cells were washed with PBS gently three times. The cells were incubated with CCK-8 working solution for 1.5 h and absorbance was measured at 450 nm.

Colony-formation assay. Concentrations of $7×10^2$ DLD1 cells and $1×10^3$ SW480 cells were seeded in 6-well plates. After incubation for 14 days, the cells were fixed in anhydrous methanol for 20 min at room temperature. Anhydrous methanol was discarded, and the cells were stained with 1% crystal violet buffer for 30 min at room temperature. The cells were washed with running water, and the colony formations were visualized.

Flow cytometry analysis. The control and sh HSPA5 DLD1 and SW480 cells were seeded in 6-well plates and treated with 20 µM erastin for 24 h. The cells were harvested and washed three times with cold PBS. The cells were resuspended in 100 µM binding buffer and gently added with 5 µM Annexin V and 5 µM propidium iodide. Then, they were incubated for 30 min at room temperature in the dark. Finally, the cells were washed thrice with binding buffer, and apoptosis was analyzed using flow cytometry (FACSCalibur, BD, New Jersey, USA).

Quantitative real-time PCR. Total RNA was extracted from the erastin-treated cells using TRIzol® reagent (15596026, Thermo, Waltham, MA, USA) according to the manufacturer's protocol. The isolated RNA was transcribed into complementary DNA using a reverse transcription kit (206143, Qiagen, Dusseldorf, Germany). A 20 µl reaction mixture was utilized under the following cycling conditions: 95 °C for 2 min, 45 cycles of 95 °C for 20 s, and 58 °C for 30 s. The dissociation step was used to generate a melting curve and to confirm the specificity of the amplification. Target gene expression was calculated using the $2^{-\Delta\Delta CT}$ method, and GAPDH was used as an internal control. The primer sequences were as follows: GAPDH, F: GACCTGCC-GTCTAGAAAAAC; R: TTGAAGTCAGAGGAGACCAC. GPX4, F: ATACGCTGAGTGTGGTTTGC; R: CTTCATC-CACTTCCACAGCG.

Lipid ROS detection. DLD1 and SW480 cells were seeded in the 6-well plates and treated with 10 µM erastin for 6 h. The cells were stained with 1.5 µM BODIPY C11 (D3861, Thermo) for 30 min in an incubator. The media was removed, and the cells were gently washed with Hanks' Balanced Salt Solution (HBSS). Trypsin (1 ml) was added to each well, and the cells were harvested. The cells were centrifuged and the medium was removed. Next, the cells were suspended with HBSS and were examined by flow cytometry (FACSCalibur, BD, New Jersey, USA).

MDA detection. MDA is a canonical product of ferroptosis. The MDA level is a good indicator of ferroptosis. The cells were harvested and lysed ~$1×10^7$ cells using 1 ml lysis buffer (P0013, Beyotime, Shanghai, China). The cells were centrifuged and the supernatant was harvested. The superna-tant (100 µl) was mixed with 200 µl of MDA working solution (S0131M, Beyotime, Shanghai, China) in a 1.5 ml centrifuge tube and heated at 100 °C for 15 min. The tubes were placed in water to cool them to room temperature. The tubes were centrifuged at 1,000×g for 10 min, and the supernatant was harvested. The supernatant (200 µl) was added to the wells of 96-well plates, and the absorbance was measured at 532 nm.

GSH detection. The kit was purchased from Beyotime (S0053). The 1.5 ml tubes were weighed, and the treated cells were harvested. The weight of the cells (1 µg of cells is equivalent to 1 µl) was calculated and M solution was added to the cells (1:3) to remove protein. The tubes were frozen and thawed twice before centrifuging at 1,000×g for 10 min at 4 °C. The supernatant was harvested to determine total GSH levels. To test glutathione disulfide (GSSG) levels, the supernatant was added to GSH scavenging adjuvants (at a ratio of 1:5) and scavengers (at a ratio of 1:25). The solution was vortexed and incubated for 60 min at the room tempera-ture to remove GSH. The sample was prepared to examine the GSSG levels. To test the total glutathione and GSSG, 10 µl of the prepared sample was added to a 150 µl working solution and incubated for 5 min at room temperature. Then, 50 µl NADPH solution (0.5 mg/ml) was added to the mixed solution, and absorbance was measured at 412 nm. The GSH level was calculated as follows: GSH = total glutathione GSSG×2.

Animal studies. Male BALB/c nude mice (4–6 weeks) were purchased from the Air Force Medical University Laboratory Animal Center. The mice were kept in the SPF environment and had free access to food and water. $3×10^6$ SW480 cells were injected subcutaneously into nude mice (n=4 or 5). Erastin was dissolved in 5% DMSO/corn oil and intraperitoneally injected into nude mice at a dose of 15 mg/kg three times [15, 16]. Three weeks later, mice were sacri-ficed and the tumors were resected and weighed. The tumors were divided into two parts. One sample was lysed and used for protein analysis. The other part was used to test for Ki67 expression. All animal procedures were approved by the experimental animal ethics committee of Tangdu Hospital.

Gene Expression Omnibus (GEO) and the Cancer Genome Atlas dataset (TCGA) analysis. The GSE39582 dataset was downloaded from Gene Expression Omnibus (https://www.ncbi.nlm.nih.gov/geo/query/acc.cgi?acc=gse39582). The dataset was analyzed using the R software (version 4.0.3). The correlation between HSPA5 and PD-1, PD-L1, IDO1, LAG3, and CTLA4 in the CRC TCGA dataset was analyzed using GEPIA2 (http://gepia2.cancer-pku.cn/#correlation) [17]. The correlation between HSPA5 and immune cell infiltration was analyzed using the TIMER2.0 (http://timer.cistrome.org/) [18].

Statistical analysis. All experimental data were analyzed as a mean estimate ± standard deviation of at least three independent replicates. The data between the two groups were compared using the Student's t-test. Data among three or more groups were compared using analysis of variance. The

$χ^2$ test was used to analyze the correlation between HSPA5 expression and clinicopathological parameters. Kaplan-Meier curves and log-rank tests were applied to explore the relationship between HSPA5 expression and overall survival. Receiver operating characteristic curve analysis was used to assess the diagnostic value of HSPA5. Statistical significance was set at p<0.05. SPSS version 19.0 was used to analyze the experimental data (Chicago, IL, USA).

Results

Unfolded protein response (UPR) was activated in ferroptosis. As a novel form of regulated cell death, ferroptosis is involved in the development of colorectal cancer [19]. Erastin is a well-known ferroptosis inducer. In our study, erastin treatment resulted in the death of DLD1 and SW480 colorectal cancer cells in a dose-dependent manner, similar to results in previous studies [20]. We tested the effects of ZVAD-FMK (apoptosis inhibitor), necrosulfonamide (necrosis inhibitor), chloroquine diphosphate (autophagy inhibitor), and ferrostatin-1 (ferroptosis inhibitor) on ferroptosis-treated cells. Consistent with the observations of previous studies, we observed that ferrostatin-1 strongly relieved the cell death induced by the erastin treatment, while ZVAD-FMK, necrosulfonamide, and chloroquine diphosphate failed to rescue the ferroptosis-treated cells (Figures 1A, 1B). It has been reported that the UPR is related to ferroptosis [13]. Our results showed that the UPR sensor IRE-1 was highly activated in a dose-dependent manner. Moreover, the downstream effectors p-eIF2α, ATF4, CHOP, and HSPA5 were also increased after treatment with erastin (Figures 1C, 1D). These results suggest that UPR is activated and has a potential regulatory role in ferroptosis.

HSPA5 protected colorectal cancer cells from erastin toxicity. UPR exerts cytoprotective or cytotoxic effects in various types of cancer. As one of the most important effectors, HSPA5 assists in maintaining target protein stability and promoting cell viability. In this study, HSPA5 expression was found to be increased in ferroptosis, indicating that HSPA5 may have a regulatory role in ferroptosis. To examine its effect on colorectal cancer cell viability, we transfected DLD1 and SW480 cells with sh-HSPA5 lentivirus and constructed the HSPA5 stably knockdown cell lines. The western blot results confirmed that HSPA5 was successfully knocked down in these two cell lines. The CCK-8 assay results validated that knockdown of HSPA5 repressed cell viability (Figures 2A, 2B). The colony formation results indicated that HSPA5 knockdown or erastin treatment repressed the colony formation ability of DLD1 and SW480 cells when compared with the control group. Moreover, the combination of HSPA5 knockdown and erastin treatment further restrained the colony formation ability of DLD1 and SW480 cells compared with the erastin treatment group or HSPA5 knockdown group (Figure 2C). An annexin V/propidium iodide assay was conducted to assess the apoptosis of DLD1 and SW480

cells. The results indicated that HSPA5 knockdown rendered DLD1 and SW480 cells more susceptible to erastin treatment (Figure 2D). Additionally, the results indicated that increased HSPA5 may represent an intrinsic protective strategy for CRC cells to resist ferroptosis. Although HSPA5 had failed to completely inhibit ferroptosis, it had attenuated erastin toxicity and supported cell growth.

HSPA5 negatively regulated ferroptosis. HSPA5 was beneficial for cell survival following erastin treatment. However, it remained unclear whether HSPA5 supported cell survival by regulating ferroptosis. Ferroptosis was characterized by excessive lipid ROS, MDA, and decreased GSH. Consistent with the results of other studies, in our study, erastin treatment induced an increase in lipid ROS compared to the DMSO group [21]. Moreover, HSPA5 knockdown exacerbated this condition and facilitated the production of more lipid ROS when compared with the erastin group (Figure 3A). MDA is the canonical product of oxidized lipids in ferroptosis. The results suggested that MDA was increased in the erastin treatment group, and HSPA5 knockdown further resulted in an increase in MDA compared with the erastin group (Figures 3B, 3C). Similarly, HSPA5 knockdown further reduced the GSH level compared to the erastin group (Figures 3D, 3E). These results confirm

Table 1. Correlation of HSPA5 expression with clinicopathological features of CRC patients in GSE39582.

Parameters	Total	HSPA5 expression			
		Low	High	$χ^2$	p-value
Gender				2.078	0.1485
Male	309	146	163		
Female	253	135	118		
Age				1.096	0.2952
<60	151	70	81		
≥60	411	211	200		
T				11.31	0.0102*
T1	11	6	5		
T2	44	32	12		
T3	364	173	191		
T4	119	53	66		
N				1.635	0.6541
N0	299	141	158		
N1	133	69	64		
N2	98	49	49		
N3	6	4	2		
M				0.08123	0.7756
M0	479	237	242		
M1	61	29	32		
TNM stage				6.645	0.0841
1	32	21	11		
2	262	119	143		
3	204	110	94		
4	60	29	31		
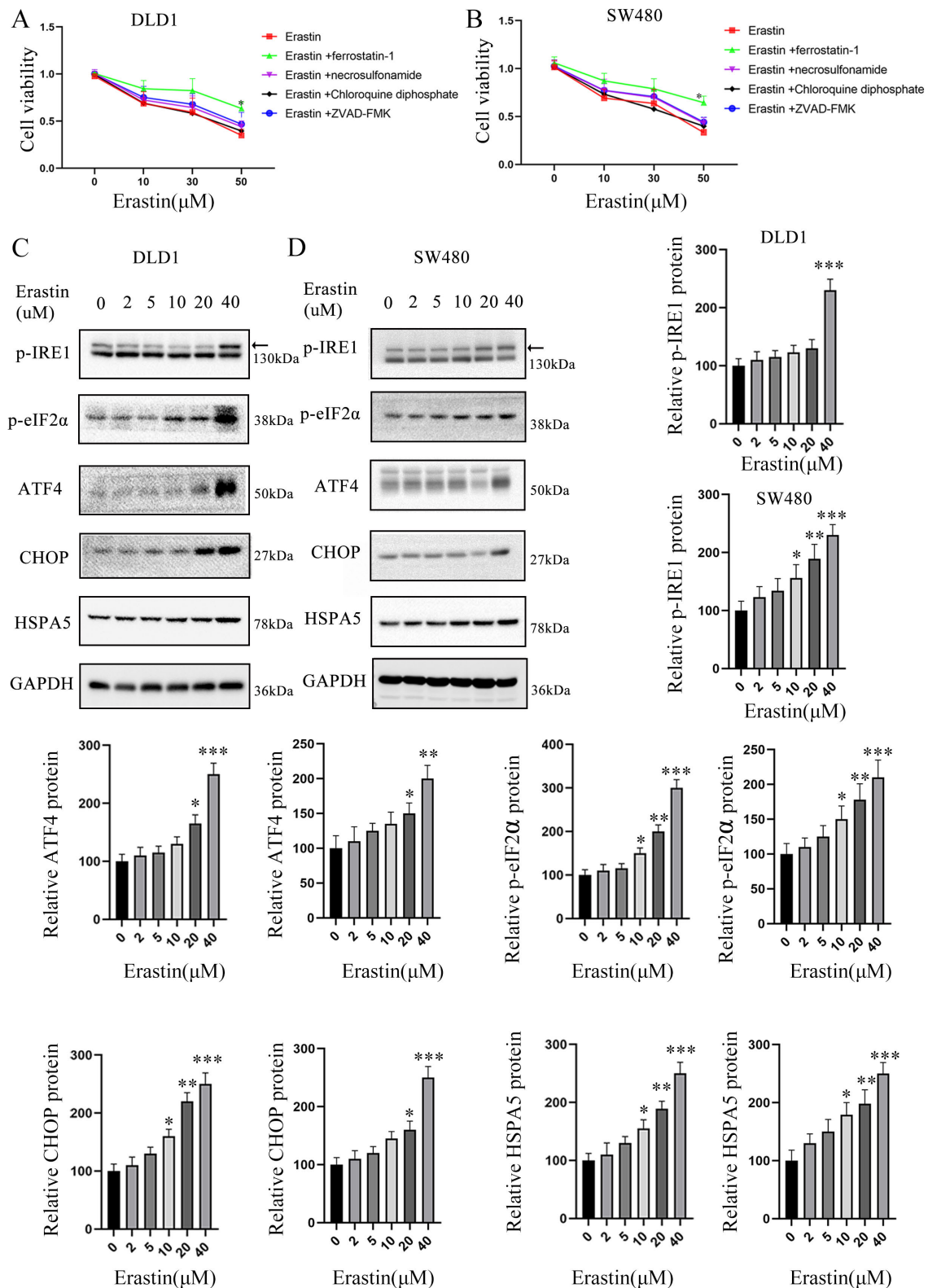
Figure 1. Unfolded protein response (UPR) was activated in ferroptosis. A, B) The CCK-8 assay result of DLD1 cells and SW480 cells after treatment with ZVAD-FMK (apoptosis inhibitor), necrosulfonamide (necrosis inhibitor), chloroquine diphosphate (autophagy inhibitor), ferrostatin-1 (ferroptosis inhibitor), and erastin, *p<0.05; C, D) The UPR-related proteins' expression of DLD1 and SW480 cells after treatment with various concentration of erastin for 24 hours (*p<0.001)**
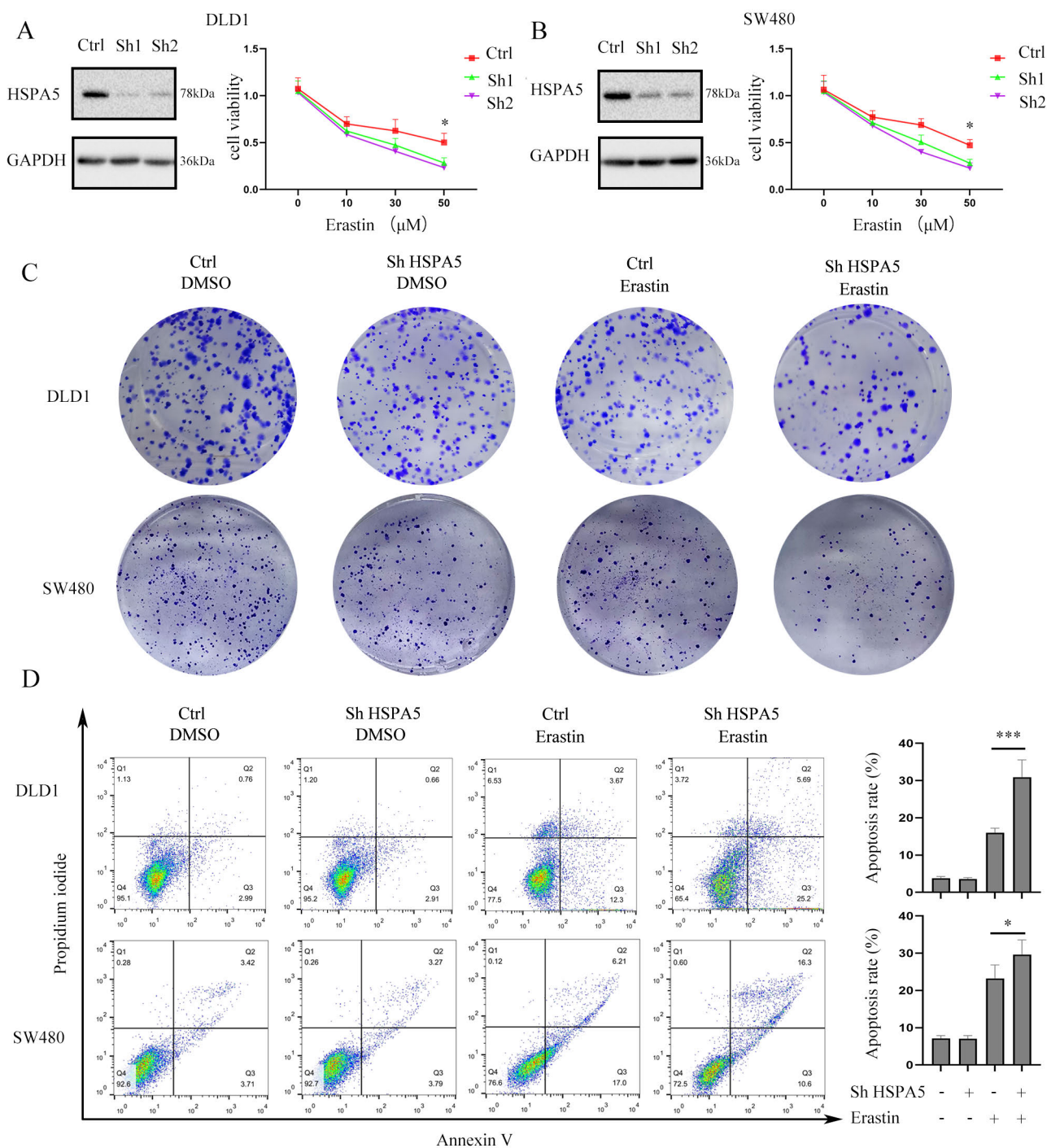
Figure 2. HSPA5 protected colorectal cancer cells from erastin toxicity. A, B) The validation of HSPA5 knockdown in DLD1 and SW480 cells and the effect of HSPA5 on cell survival when treated with erastin, *p<0.05. C) The effect of HSPA5 on DLD1 (the upper figures) and SW480 cells (the lower figures) colony formation ability. D) The effect of HSPA5 on DLD1 (the upper ones) and SW480 cells (the lower ones) apoptosis when treated with erastin. 10,000 cells were analyzed in each group, *p<0.05, ***p<0.001

that HSPA5 negatively modulated ferroptosis of CRC cells when treated with erastin.

HSPA5 bound to GPX4 and maintained its stability. We examined the molecular mechanism of HSPA5 in regulating

ferroptosis. GPX4 is one of the most critical regulators of ferroptosis. Previous studies have reported that HSPA5 maintains GPX4 stability in pancreatic cancer and glioma [12, 13]. However, its role in CRC remains relatively unclear.
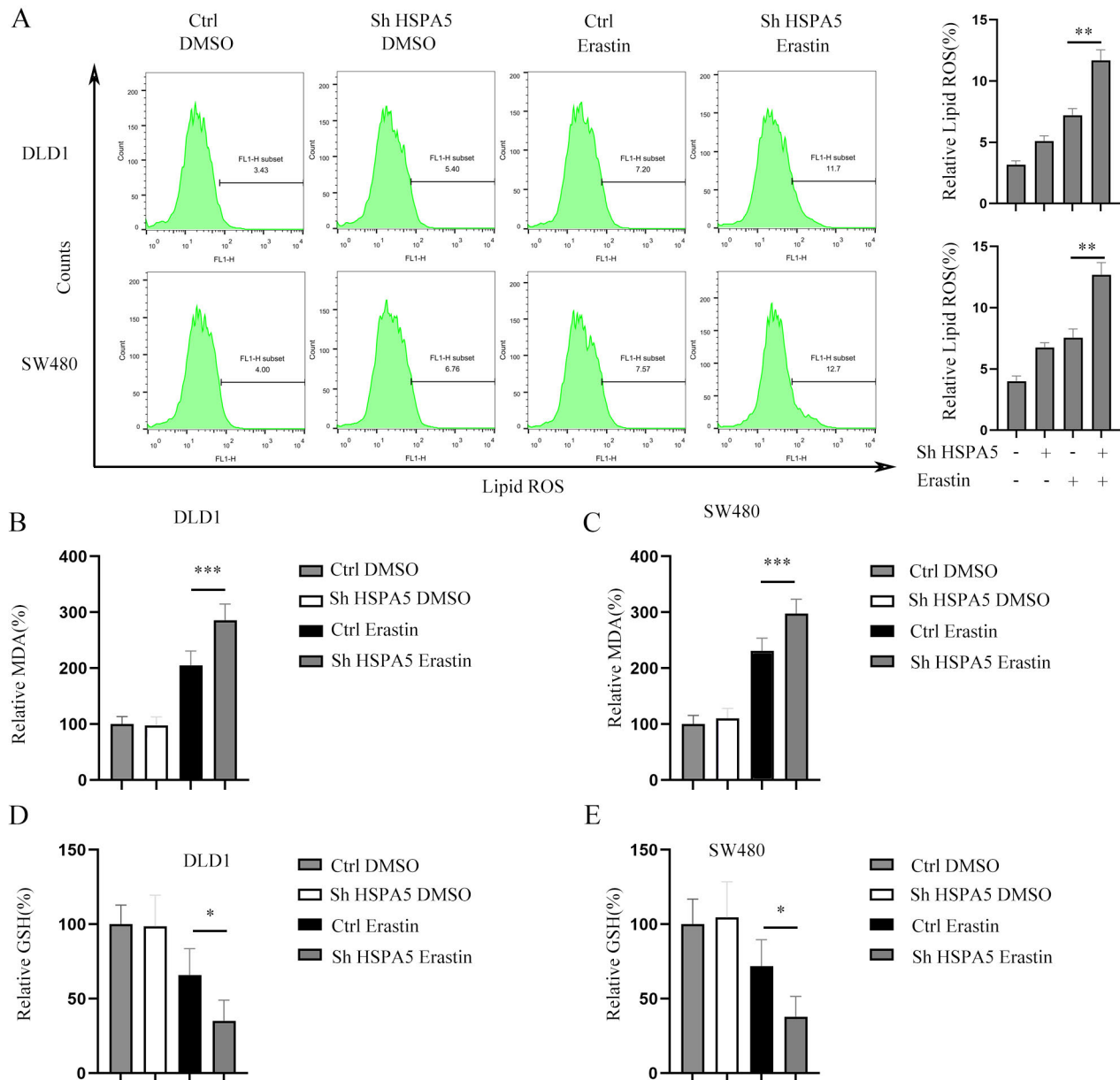
Figure 3. HSPA5 negatively regulated ferroptosis. A) The effect of HSPA5 on lipid ROS production of DLD1 (the upper ones) and SW480 cells (the lower ones) when treated with erastin, **p<0.01; **B, C)** The effect of HSPA5 on MDA production of DLD1 and SW480 cells after erastin treatment, ***p<0.001; **D, E)** The effect of HSPA5 on the GSH level in erastin-treated DLD1 and SW480 cells, *p<0.05

In our study, erastin treatment had little effect on GPX4 mRNA expression (Figures 4A, 4B), which was consistent with previous studies. However, erastin treatment repressed GPX4 protein in a dose-dependent manner (Figures 4C, 4D). These results confirmed that erastin modulated GPX4 protein stability but not GPX4 protein synthesis. Furthermore, we examined the effect of HSPA5 on GPX4 protein levels. The results disclosed that GPX4 was decreased, whereas HSPA5 expression was increased in control cells when treated with erastin. Moreover, GPX4 was further decreased in HSPA5 knockdown cells (Figures 4E, 4F) compared with the control group. The results demonstrated that HSPA5 retarded the erastin-induced GPX4 decrease and assisted in maintaining GPX4 stability.

Additionally, we explored the underlying mechanisms by immunoprecipitating HSPA5 and found that it is directly bound to GPX4 (Figure 5A). Likewise, we proved that GPX4 directly bound to HSPA5 by immunoprecipitating GPX4 and

examined HSPA5 (Figure 5B). As a chaperone molecule, HSPA5 has been shown to bind to and stabilize the target protein. For HSPA5 negatively regulating ferroptosis, we explored the effect of erastin on HSPA5 binding ability with GPX4. As shown in Figures 5C and 5D, cells were exposed to 10 or 20 μM erastin for a short period of time (8 h). The results suggested that the interaction between HSPA5 and GPX4 increased in a dose-dependent manner. Combined with the results in Figure

4, we deduced that HSPA5 was directly bound to GPX4 and maintained its stability. Although the interaction between HSPA5 and GPX4 failed to completely reverse the erastin-induced GPX4 decrease, HSPA5 slowed down the GPX4 degradation process and alleviated ferroptosis. Increasing HSPA5 could be an intrinsic protective strategy to resist ferroptosis. It provides cells with more time to adapt to ferroptosis, despite the cells ultimately suffering from ferroptosis.
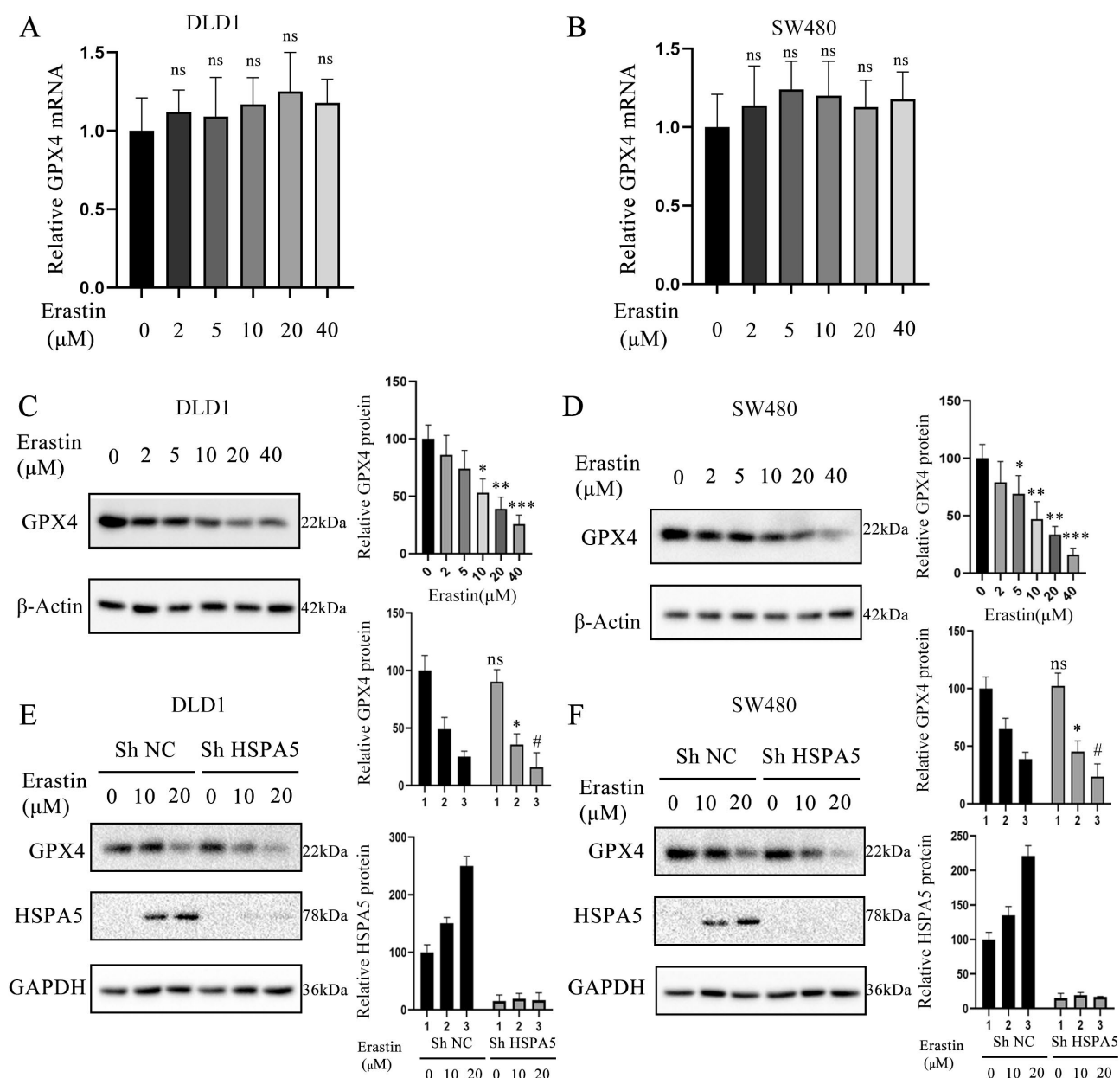
Figure 4. HSPA5 maintained the stability of GPX4. A, B) The mRNA expression of GPX4 of DLD1 and SW480 cells after treatment with various concentration of erastin; **C, D)** The protein expression of GPX4 of DLD1 and SW480 cells after treatment with erastin, *p<0.05, **p<0.01, ***p<0.001; **E, F)** The effect of HSPA5 on GPX4 protein expression in DLD1 and SW480 cells when treated with erastin, *p<0.05 compared with control cells treated with 10 μM erastin, #p<0.05 compared with control cells treated with 20 μM erastin

HSPA5 knockdown sensitized CRC tumor to erastin treatment *in vivo*. To confirm the HSPA5 effect on ferroptosis *in vivo*, the HSPA5 knockdown SW480 cells were subcutaneously injected into the nude mice. The results showed that erastin treatment decreased tumor weight when compared with the corresponding control group. The combination of HSPA5 knockdown and erastin treatment further suppressed tumor development in SW480 cells when compared with the erastin group (Figures 6A, 6B). The results confirmed that HSPA5 knockdown made SW480 cells more susceptible to erastin treatment. Ki67 staining was subsequently conducted to examine the proliferative ability of the tumors. The results confirmed that HSPA5 knockdown or erastin treatment both decreased cell proliferation ability in SW480 when compared with the control group, and the combination of the HSPA5 knockdown and erastin treatment further inhibited tumor proliferation (Figure 6C). We also examined HSPA5 and GPX4 expression in these samples. The results suggested that

HSPA5 was increased and GPX4 was decreased in the erastin group when compared with the control group. The combination of HSPA5 knockdown and erastin treatment further induced a GPX4 decrease when compared with the erastin group. The *in vivo* results confirmed that the HSPA5 knockdown sensitized CRC tumors to erastin treatment, which was consistent with the *in vitro* results (Figure 6D).

HSPA5 was correlated with ferroptosis in CRC patients. To explore the effect of HSPA5 on ferroptosis in CRC patients, we first analyzed the expression of HSPA5 and GPX4 in CRC tissues and corresponding normal tissues. The results illustrated that HSPA5 and GPX4 were both increased in CRC tissues compared to normal tissues (Figure 7A). To further verify the relationship between HSPA5 and ferroptosis, we downloaded the CRC dataset (GSE39582) from The Cancer Genome Atlas and analyzed the HSPA5 expression. The results confirmed that HSPA5 was highly expressed in CRC tissue compared to normal tissue (Figure 7B). Further-
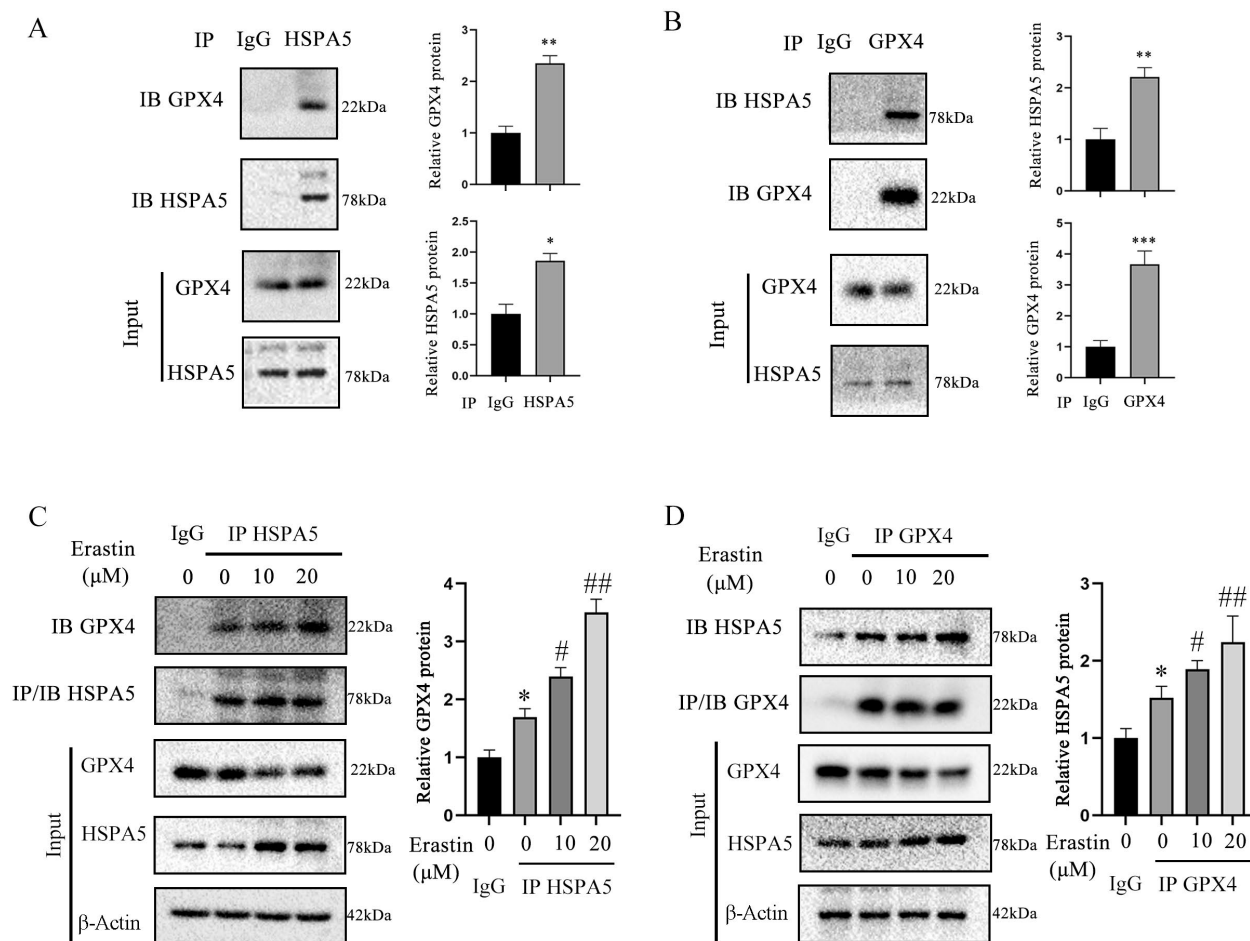
Figure 5. HSPA5 directly bound to GPX4. A) GPX4 directly bound to HSPA5 when immune-precipitated with HSPA5 protein in DLD1 cells, *p<0.05, **p<0.01; **B)** HSPA5 directly bound to GPX4 when immune-precipitated with GPX4 protein in DLD1 cells, **p<0.01, ***p<0.001; **C, D)** The binding between GPX4 and HSPA5 was increased when treated with erastin in DLD1 cells, *p<0.05 compared with the IgG group, #p<0.05 and ##p<0.01 compared with IP HSPA5 cells without erastin treatment

more, we found that HSPA5 expression was correlated with advanced T stage (p<0.05), but not with gender, age, N stage, or TNM stage (Table 1). Consistently, the patients with high HSPA5 expression had the worse overall survival (Figure 7C). The univariate analysis suggested that HSPA5 can be used as a prognostic indicator for CRC patients (Figure 7D). Furthermore, we analyzed the relationship between HSPA5 and ferroptosis-related gene signature. The result showed that HSPA5 was related to the expression of ferroptosis-related gene signature, indicating HSPA5 was a potential modulator of ferroptosis in CRC patients (Figure 7E). These results hint that HSPA5 promotes tumor development in CRC patients, partly by regulating ferroptosis.

HSPA5 was associated with the tumor immune microenvironment in CRC. It has been shown that ferroptosis regulates the tumor microenvironment and predicts immunotherapy response in cancers [22]. Our results confirmed that HSPA5 negatively modulated ferroptosis,

then we aimed to explore the correlation between HSPA5 and tumor immune microenvironment. As shown in Figure 8, HSPA5 expression was positively related to that of PD-L1, PD-1, CTLA4, IDO1, and LAG3, which play immune-suppressive roles in cancer development (Figures 8A–8E) [23–25]. Additionally, we analyzed the correlation of HSPA5 with immune cell infiltration. Cytotoxic T cells (CD8+ T cells) were the primary anti-tumor immune cells [21]. The results showed that HSPA5 was negatively related to CD8+ T cell level (Figure 8F). Regulatory T cells (Treg cells) are one of the most critical immune-suppressive immune cells, which promote cancer progression [27]. The result suggested that HSPA5 was positively related to Treg cell level (Figure 8G). Increased cancer-associated fibroblasts (CAF) were revealed to repress immune cell infiltration [28]. Consistently, HSPA5 was positively related to the CAF level (Figure 8H). These results implied that HSPA5 was associated with the immune microenvironment in CRC.
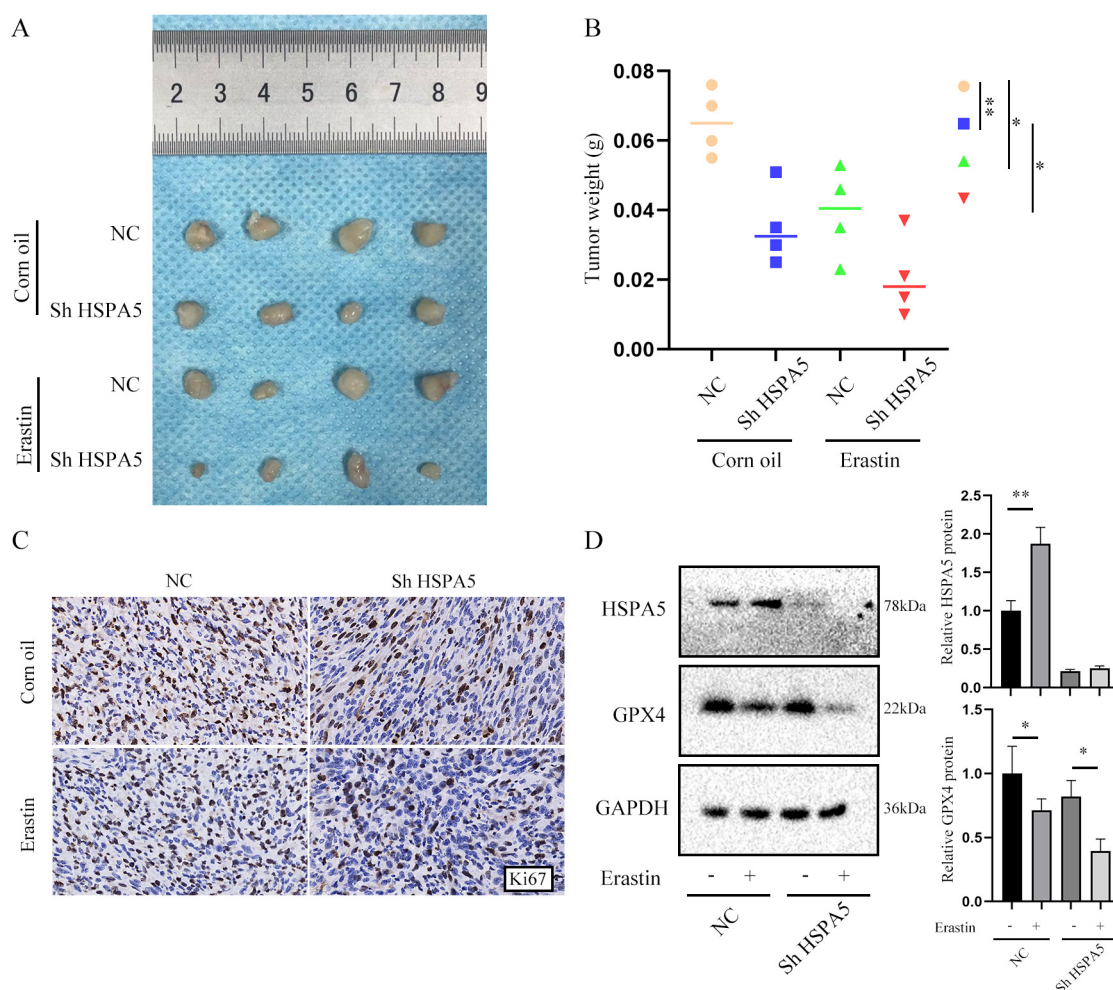
Figure 6. HSPA5 promoted tumor development under the erastin treatment *in vivo*. A) The subcutaneous tumors of nude mice were separated and photographed; **B)** The weight of subcutaneous tumors in indicated groups, *p<0.05, **p<0.01; **C)** The Ki67 staining of each group; **D)** The expression of HSPA5 and GPX4 proteins in subcutaneous tumors, *p<0.05, **p<0.01
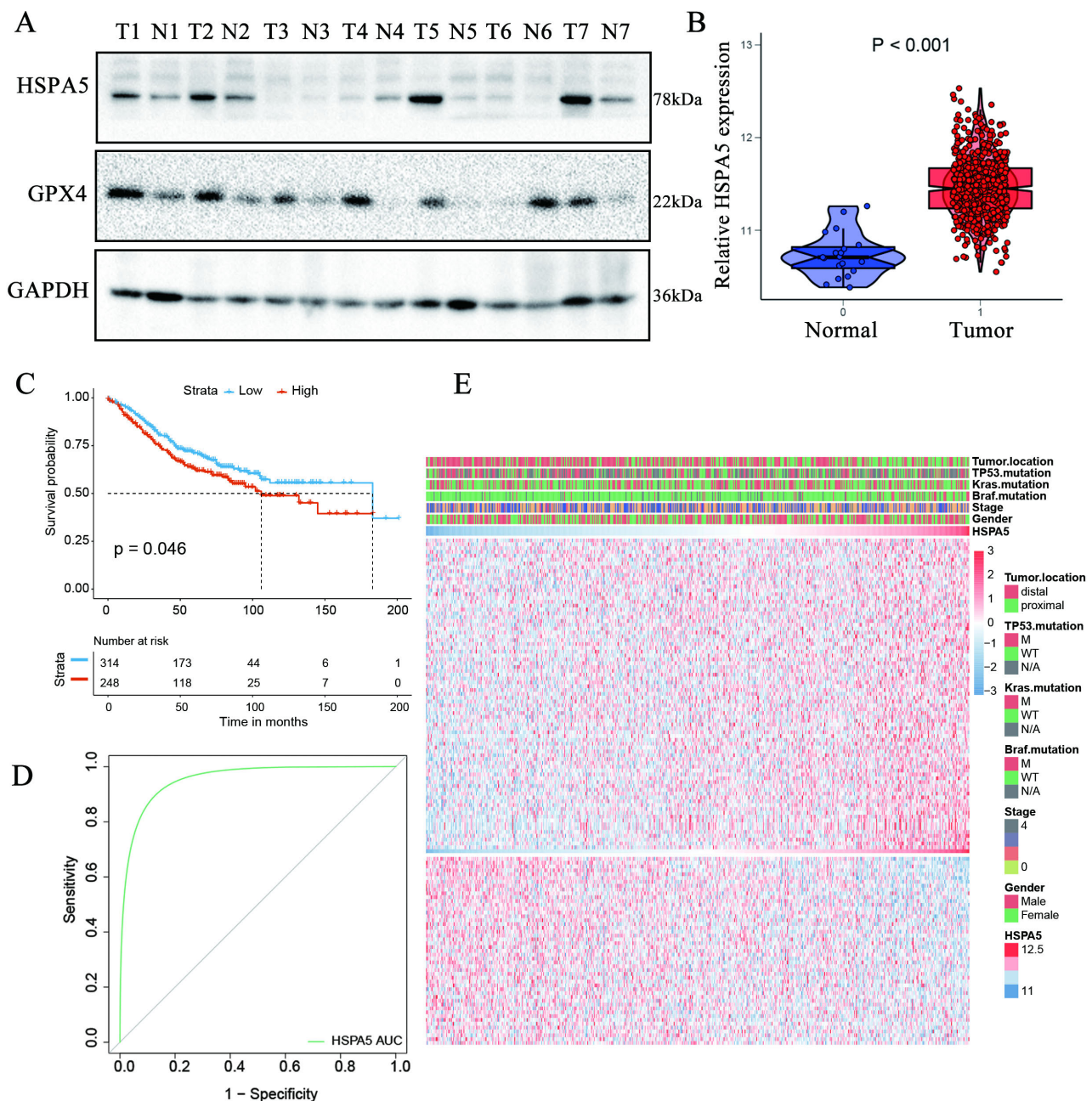
Figure 7. HSPA5 was correlated with ferroptosis in CRC patients. A) The HSPA5 and GPX4 protein expression in CRC tissues and corresponding normal tissues; **B)** The expression of HSPA5 in CRC tissues and normal tissues in GSE39582, p<0.001; **C)** The OS of patients with high HSPA5 expression or low HSPA5 expression, p<0.05; **D)** The ROC curve analysis of HSPA5 (AUC=0.954); **E)** The heatmap of correlation between HSPA5 with ferroptosis.

Discussion

CRC is one of the most prevalent malignant cancers worldwide. Despite multiple therapeutic strategies, the prognosis of CRC patients is yet poor. One of the main reasons is the lack of understanding of the pathological mechanisms of CRC. Ferroptosis is a newly discovered and defined regulated cell death that has been shown to participate in the development of various cancers [19, 29]. This study revealed an intrinsic

protective pathway to resist ferroptosis in CRC. We found that UPR was activated and HSPA5 was increased during the induction of ferroptosis. As one of the most common and critical effector proteins of the UPR, HSPA5 attenuated the erastin-induced GPX4 decrease, repressed ferroptosis, and promoted CRC growth *in vitro* and *in vivo*. Mechanistically, HSPA5 bound directly to GPX4 and increased its stability. The interaction between HSPA5 and GPX4 slowed down the

GPX4 degradation process. Our study disclosed that HSPA5 negatively regulated ferroptosis to promote CRC development by increasing GPX4 stability (Figure 9) and provided a potential diagnostic and therapeutic biomarker for CRC.

When cells are confronted with detrimental stimuli or environments, complex responses occur in the intracellular space. Some responses are directly caused by the detrimental stimulus, which activated the apoptosis-related pathways and promoted cell death. For example, the erastin treatment induces Nedd4 expression, which promotes VDAC2/3

degradation and induces ferroptosis [30]. Meanwhile, the cells develop intrinsic protective strategies to resist harmful environments and support cell survival. Erastin treatment has been reported to induce NRF2 expression, which transcriptionally upregulates cystathionine β-synthase and represses ferroptosis. It is one of the canonical intrinsic pathways of cells to resist ferroptosis [31]. Enhancement of harmful pathways or inhibition of intracellular protective pathways is a potential strategy to sensitize cells to ferroptosis [32, 33].
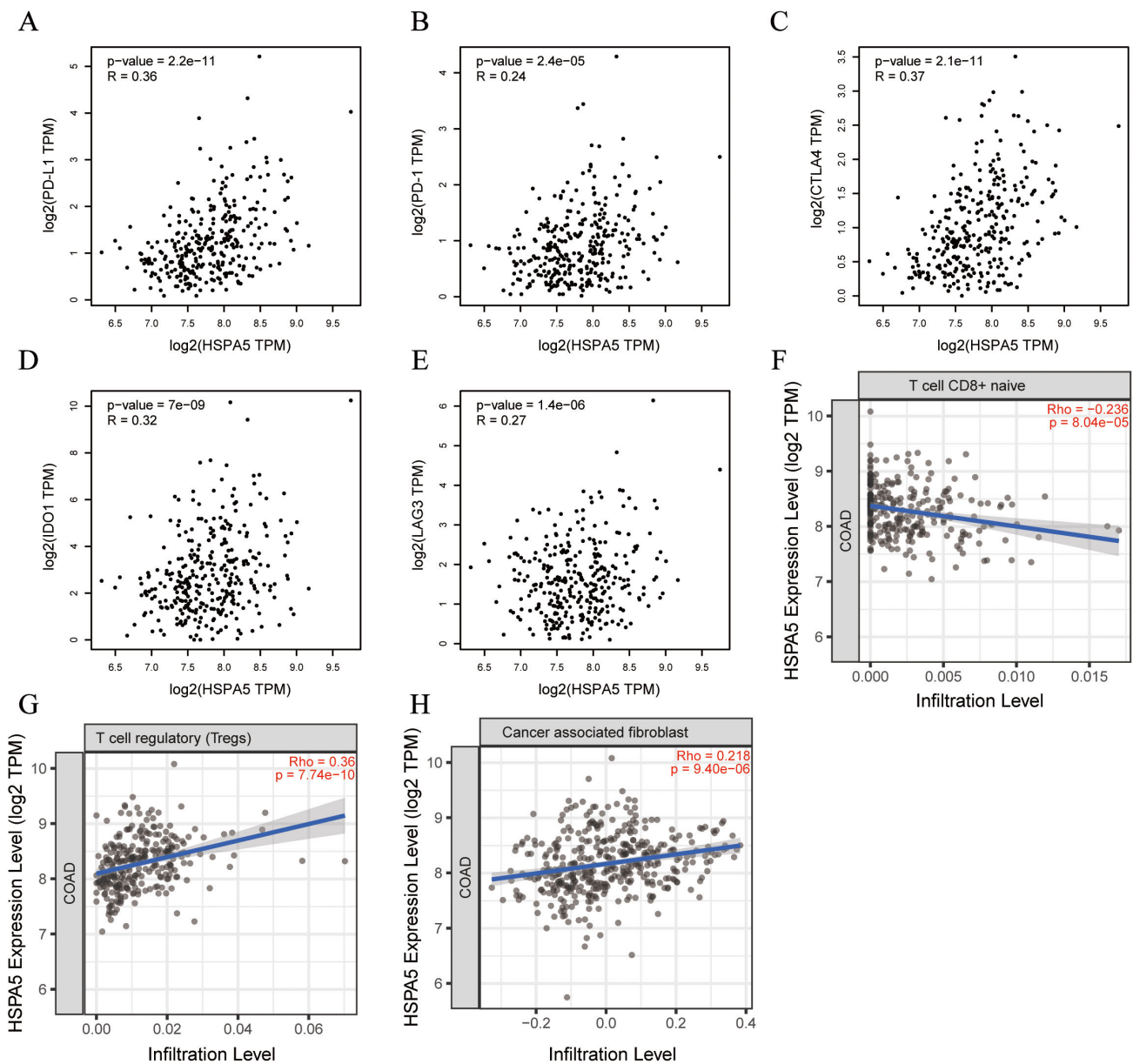
Figure 8. HSPA5 was associated with the tumor immune microenvironment in CRC. A–E) The correlation of HSPA5 with PD-L1, PD-1, CTLA4, IDO1, and LAG3 in the CRC TCGA dataset, respectively; **F-H)** The correlation of HSPA5 with CD8$^+$ T cell, Treg cell, and CAF infiltration level in the CRC TCGA dataset, respectively.

UPR is a physiological or pathological cellular activity that promotes cell survival or apoptosis, depending on various extracellular and intracellular environments. UPR sensors are composed of three signal transducers – PERK, IRE1, and ATF6 [34, 35]. There are many downstream effectors of these three signaling pathways, and HSPA5 is one of the key and shared effectors. The UPR can be activated by different stimuli, such as altered redox status, accumulation of misfolded proteins, energy deprivation, calcium homeostasis, and dysregulation of non-coding RNAs, which all result in UPR activation [36]. Ferroptosis is characterized by the exhaustion of GSH and accumulation of oxidized lipids, which inhibits cell survival and represses tumor development [37]. However, the correlation between UPR and ferroptosis has not been fully elucidated in CRC. This study found that the ferroptosis inducer erastin activated UPR in CRC cells. UPR has complex functions in different contexts. These results suggest that UPR is involved in ferroptosis. However, whether UPR is a detrimental or protective pathway for ferroptosis remains to be explored.

HSPA5 is a central effector of UPR. HSPA5 is highly expressed when UPR is activated. HSPA5 dissociated from PERK or IRE1 to initiate UPR. Additionally, HSPA5 binds to target proteins to promote their correct folding or maintain their stability [38, 39]. To examine the specific role of HSPA5 in CRC cells, we knocked down HSPA5 and treated cells with the ferroptosis inducer erastin. We found that knockdown of HSPA5 had a synergistic effect with erastin to inhibit cell viability. These results indicate that HSPA5 was beneficial for cell survival. HSPA5 has been shown to regulate the immune response, autophagy, and apoptosis in controlling cell viability [40–42]. Then we tried to explore whether HSPA5 protects cells by modulating ferroptosis. The exhaustion of GSH and overproduction of lipid ROS and MDA are indicators of ferroptosis. We found that HSPA5 knockdown decreased the GSH pool and increased lipid ROS and MDA production, indicating that HSPA5 negatively regulates ferroptosis in CRC cells when treated with erastin.

Ferroptosis has been extensively studied in CRC. For instance, GPX4 inactivation and ROS production have been shown to inhibit CRC cell proliferation [19]. Resibufogenin was also reported to inhibit ferroptosis in CRC by inactivating GPX4 [43]. By modulating GSH levels, GPX4 is one of the most important regulators of ferroptosis. In pancreatic cancer, HSPA5 has been shown to interact with GPX4 and stabilize GPX4 [13]. However, it is unknown whether HSPA5 plays a regulatory role in GPX4 in CRC. In this study,
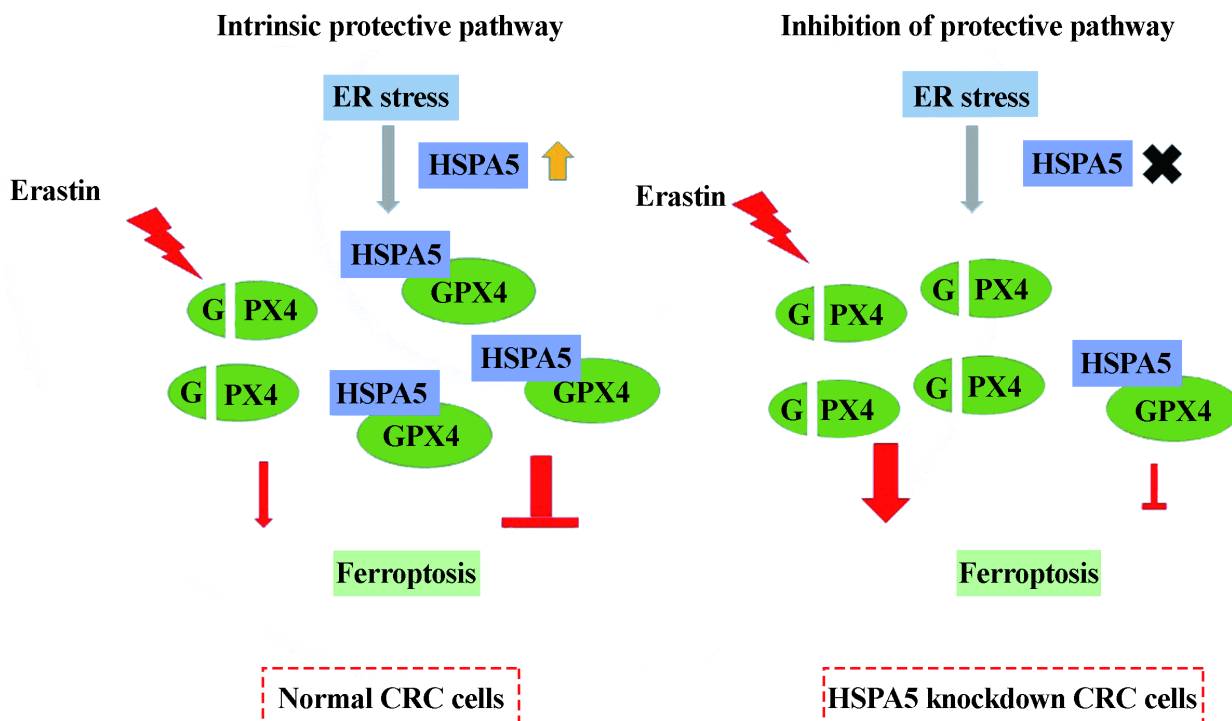
Figure 9. Graphical abstract of HSPA5 negatively regulated ferroptosis to promote colorectal cancer development via maintaining GPX4 stability. As shown on the left side of the diagram, in the control CRC cells, erastin treatment induced the GPX4 degradation and ferroptosis. In order to survive, CRC cells developed the intrinsic strategy to resist erastin toxicity. UPR was activated and HSPA5 was increased after erastin treatment. The increased HSPA5 directly bound to GPX4 and slowed down its degradation process. Though the effect of HSPA5 was limited, it gave CRC cells more time to adjust to the detrimental environment. As shown on the right side of the diagram, when the HSPA5 was knocked down, GPX4 was more likely to be degraded after erastin treatment for the lack of the protective effect of HSPA5. The HSPA5 knockdown cells were more sensitive to erastin and ferroptosis.

we demonstrated that erastin treatment induced the GPX4 decrease, which is consistent with the results of previous studies [16, 44]. Moreover, the HSPA5 knockdown further promoted erastin-induced GPX4 decrease, suggesting that HSPA5 assisted in maintaining GPX4 stability when CRC cells were treated with erastin. Mechanistically, we demonstrated that HSPA5 directly binds to GPX4. The interaction between HSPA5 and GPX4 was enhanced when treated with erastin for a short time period. We deduced that increased HSPA5 was an intrinsic protective strategy to resist ferroptosis. HSPA5 was increased to bind GPX4 and slow down its degradation process. Although HSPA5 has failed to completely reverse the GPX4 decrease and inhibit ferroptosis, it provided cells with more time to adapt to the detrimental environment. Therefore, by inhibiting HSPA5, an effective strategy can be introduced to hinder the intracellular protective pathway and make CRC cells more susceptible to ferroptosis.

Ferroptosis has been reported to regulate the tumor immune microenvironment [45]. In the present study, we confirmed that HSPA5 was related to increased expression of immune-relevant genes. Moreover, HSPA5 was related to immune cell infiltration. These results implied that HSPA5 played an important role in regulating the immune microenvironment. Targeting HSPA5 is a potential strategy to improve the immunotherapy response in CRC. We deduced that HSPA5 modulated the immune microenvironment partly by regulating ferroptosis. More studies are required to verify this hypothesis and explore more underlying mechanisms.

However, the effect of increased HSPA5 was limited when cells were treated with high concentrations of erastin for a long period. These results hinted that HSPA5 was only one of the intracellular protective mechanisms to resist ferroptosis. Although targeting HSPA5 is a potential strategy to sensitize cells to ferroptosis, more research efforts are urgently required to unravel more pathological mechanisms underlying ferroptosis resistance.

In this study, we found that UPR was activated in ferroptosis and that the UPR effector HSPA5 negatively modulated ferroptosis by stabilizing the GPX4 protein. Our study discovered a novel mechanism accounting for CRC development, thus, providing a prognostic and therapeutic target for CRC patients.

References

[1]   SIEGEL RL, MILLER KD, GODING SAUER A, FEDEWA SA, BUTTERLY LF et al. Colorectal cancer statistics, 2020. CA Cancer J Clin 2020; 70: 145–164. https://doi.org/10.3322/caac.21601

[2]   GUINNEY J, DIENSTMANN R, WANG X, DE REYNIES A, SCHLICKER A et al. The consensus molecular subtypes of colorectal cancer. Nat Med 2015; 21: 1350–1356. https://doi.org/10.1038/nm.3967

[3]   DIXON SJ, LEMBERG KM, LAMPRECHT MR, SKOUTA R, ZAITSEV EM et al. Ferroptosis: an iron-dependent form of nonapoptotic cell death. Cell 2012; 149: 1060–1072. https://doi.org/10.1016/j.cell.2012.03.042

[4]   LI J, CAO F, YIN HL, HUANG ZJ, LIN ZT et al. Ferroptosis: past, present and future. Cell Death Dis 2020; 11: 88. https://doi.org/10.1038/s41419-020-2298-2

[5]   LI C, DENG X, ZHANG W, XIE X, CONRAD M et al. Novel Allosteric Activators for Ferroptosis Regulator Glutathione Peroxidase 4. J Med Chem 2019; 62: 266–275. https://doi.org/10.1021/acs.jmedchem.8b00315

[6]   JIA M, QIN D, ZHAO C, CHAI L, YU Z et al. Redox homeostasis maintained by GPX4 facilitates STING activation. Nat Immunol 2020; 21: 727–735. https://doi.org/10.1038/s41590-020-0699-0

[7]   SONG X, WANG X, LIU Z, YU Z. Role of GPX4-Mediated Ferroptosis in the Sensitivity of Triple Negative Breast Cancer Cells to Gefitinib. Front Oncol 2020; 10: 597434. https://doi.org/10.3389/fonc.2020.597434

[8]   DING C, DING X, ZHENG J, WANG B, LI Y et al. 532 miR-182-5p and miR-378a-3p regulate ferroptosis in I/R-induced renal injury. Cell Death Dis 2020; 11: 929. https://doi.org/10.1038/s41419-020-03135-z

[9]   HOU Y, CAI S, YU S, LIN H. Metformin induces ferroptosis by targeting miR-324-3p/GPX4 axis in breast cancer. Acta Biochim Biophys Sin (Shanghai) 2021; 53: 333–341. https://doi.org/10.1093/abbs/gmaa180

[10]   COLEMAN OI, HALLER D. ER Stress and the UPR in Shaping Intestinal Tissue Homeostasis and Immunity. Front Immunol 2019; 10: 2825. https://doi.org/10.3389/fimmu.2019.02825

[11]   WANG J, LEE J, LIEM D, PING P. HSPA5 Gene encoding Hsp70 chaperone BiP in the endoplasmic reticulum. Gene 2017; 618: 14–23. https://doi.org/10.1016/j.gene.2017.03.005

[12]   ZHU S, ZHANG Q, SUN X, ZEH HJ, 3RD, LOTZE MT et al. HSPA5 Regulates Ferroptotic Cell Death in Cancer Cells. Cancer Res 2017; 77: 2064–2077. https://doi.org/10.1158/0008-5472.CAN-16-1979

[13]   CHEN Y, MI Y, ZHANG X, MA Q, SONG Y et al. Dihydroartemisinin-induced unfolded protein response feedback attenuates ferroptosis via PERK/ATF4/HSPA5 pathway in glioma cells. J Exp Clin Cancer Res 2019; 38: 402. https://doi.org/10.1186/s13046-019-1413-7

[14]   LEE SJ, LEE I, LEE J, PARK C, KANG WK. Statins, 3-hydroxy-3-methylglutaryl coenzyme A reductase inhibitors, potentiate the anti-angiogenic effects of bevacizumab by suppressing angiopoietin2, BiP, and Hsp90alpha in human colorectal cancer. Br J Cancer 2014; 111: 497–505. https://doi.org/10.1038/bjc.2014.283

[15]   LUO M, WU L, ZHANG K, WANG H, ZHANG T et al. miR-137 regulates ferroptosis by targeting glutamine t ransporter SLC1A5 in melanoma. Cell Death Differ 2018; 25: 1457–1472. https://doi.org/10.1038/s41418-017-0053-8

[16] SHIBATA Y, YASUI H, HIGASHIKAWA K, MIYAMOTO N, KUGE Y. Erastin, a ferroptosis-inducing agent, sensitized cancer cells to X-ray irradiation via glutathione starvation in vitro and in vivo. PLoS One 2019; 14: e0225931. https://doi.org/10.1371/journal.pone.0225931

[17] TANG Z, KANG B, LI C, CHEN T, ZHANG Z. GEPIA2: an enhanced web server for large-scale expression profiling and interactive analysis. Nucleic Acids Res 2019; 47: W556–W560. https://doi.org/10.1093/nar/gkz430

[18] LI T, FU J, ZENG Z, COHEN D, LI J et al. TIMER2.0 for analysis of tumor-infiltrating immune cells. Nucleic Acids Res 2020; 48: W509–W514. https://doi.org/10.1093/nar/gkaa407

[19] SUI X, ZHANG R, LIU S, DUAN T, ZHAI L et al. RSL3 Drives Ferroptosis Through GPX4 Inactivation and ROS Production in Colorectal Cancer. Front Pharmacol 2018; 9: 1371. https://doi.org/10.3389/fphar.2018.01371

[20] WANG R, SU Q, YIN H, WU D, LV C et al. Inhibition of SRSF9 enhances the sensitivity of colorectal cancer to erastin-induced ferroptosis by reducing glutathione peroxidase 4 expression. Int J Biochem Cell Biol 2021; 134: 105948. https://doi.org/10.1016/j.biocel.2021.105948

[21] ZHANG Z, GUO M, LI Y, SHEN M, KONG D et al. RNA-binding protein ZFP36/TTP protects against ferroptosis by regulating autophagy signaling pathway in hepatic stellate cells. Autophagy 202; 16: 1482–1505. https://doi.org/10.1080/15548627.2019.1687985

[22] LUAN JC, ZENG TY, ZHANG QJ, XIA DR, CONG R et al. A novel signature constructed by ferroptosis-associated genes (FAGs) for the prediction of prognosis in bladder urothelial carcinoma (BLCA) and associated with immune infiltration. Cancer Cell Int 2021; 21: 414. https://doi.org/10.1186/s12935-021-02096-3

[23] ANDREWS LP, YANO H, VIGNALI DAA. Inhibitory receptors and ligands beyond PD-1, PD-L1 and CTLA-4: breakthroughs or backups. Nat Immunol 2019; 20: c1425–1434. https://doi.org/10.1038/s41590-019-0512-0

[24] ANDREWS LP, MARCISCANO AE, DRAKE CG, VIGNALI DA. LAG3 (CD223) as a cancer immunotherapy target. Immunol Rev 2017; 276: 80–96. https://doi.org/10.1111/imr.12519

[25] ZHAI L, LADOMERSKY E, LENZEN A, NGUYEN B, PATEL R et al. IDO1 in cancer: a Gemini of immune checkpoints. Cell Mol Immunol 2018; 15: 447–457. 586 https://doi.org/10.1038/cmi.2017.143

[26] IWAHORI K. Cytotoxic CD8(+) Lymphocytes in the Tumor Microenvironment. Adv Exp Med Biol 2020; 1224: 53–62. https://doi.org/10.1007/978-3-030-35723-8_4

[27] WHITESIDE TL. FOXP3+ Treg as a therapeutic target for promoting anti-tumor immunity. Expert Opin Ther Targets 2018; 22: 353–363. https://doi.org/10.1080/14728222.2018.1451514

[28] LIU T, HAN C, WANG S, FANG P, MA Z et al. 591 Cancer-associated fibroblasts: an emerging target of anti-cancer immunotherapy. J Hematol Oncol 2019; 12: 86. https://doi.org/10.1186/s13045-019-0770-1

[29] CHEN P, LI X, ZHANG R, LIU S, XIANG Y et al. Combinative treatment of beta-elemene and cetuximab is sensitive to KRAS mutant colorectal cancer cells by inducing ferroptosis and inhibiting epithelial-mesenchymal transformation. Theranostics 2020; 10: 5107–5119. https://doi.org/10.7150/thno.44705

[30] YANG Y, LUO M, ZHANG K, ZHANG J, GAO T et al. Nedd4 ubiquitylates VDAC2/3 to suppress erastin-induced ferroptosis in melanoma. Nat Commun 2020; 11: 433. https://doi.org/10.1038/s41467-020-14324-x

[31] LIU N, LIN X, HUANG C. Activation of the reverse trans-sulfuration pathway through NRF2/CBS confers erastin-induced ferroptosis resistance. Br J Cancer 2020; 122: 279–292. https://doi.org/10.1038/s41416-019-0660-x

[32] BROWN CW, AMANTE JJ, CHHOY P, ELAIMY AL, LIU H et al. Mercurio AM (2019) Prominin2 Drives Ferroptosis Resistance by Stimulating Iron Export. Dev Cell 2019; 51: 575–586 e4. https://doi.org/10.1016/j.devcel.2019.10.007

[33] FU D, WANG C, YU L, YU R. Induction of ferroptosis by ATF3 elevation alleviates cisplatin resistance in gastric cancer by restraining Nrf2/Keap1/xCT signaling. Cell Mol Biol Lett 2021; 26: 26. https://doi.org/10.1186/s11658-021-00271-y

[34] URRA H, DUFEY E, AVRIL T, CHEVET E, HETZ C. Endoplasmic Reticulum Stress and the Hallmarks of Cancer. Trends Cancer 2016; 2: 252–262. https://doi.org/10.1016/j.trecan.2016.03.007

[35] HETZ C, PAPA FR. The Unfolded Protein Response and Cell Fate Control. Mol Cell 2018; 69: 169–181. https://doi.org/10.1016/j.molcel.2017.06.017

[36] FLAHERTY DP, GOLDEN JE, LIU C, HEDRICK M, GOSALIA P et al. Selective small molecule activator of the apoptotic arm of the UPR. In: Probe Reports from the NIH Molecular Libraries Program [Eds.]. Bethesda (MD): National Center for Biotechnology Information (US); 2010. [As available online 2013 Feb 28] https://www.ncbi.nlm.nih.gov/books/NBK133431/

[37] WANG W, GREEN M, CHOI JE, GIJON M, KENNEDY PD et al. CD8(+) T cells regulate tumour ferroptosis during cancer immunotherapy. Nature 2019; 569: 270–274. https://doi.org/10.1038/s41586-019-1170-y

[38] KIM SY, KIM HJ, KIM HJ, KIM DH, HAN JH et al. HSPA5 negatively regulates lysosomal activity through ubiquitination of MUL1 in head and neck cancer. Autophagy 2018, 14: 385–403. https://doi.org/10.1080/15548627.2017.1414126

[39] MU N, LEI Y, WANG Y, WANG Y, DUAN Q et al. Inhibition of SIRT1/2 upregulates HSPA5 acetylation and induces pro-survival autophagy via ATF4-DDIT4-mTORC1 axis in human lung cancer cells. Apoptosis 2019; 24: 798–811. https://doi.org/10.1007/s10495-019-01559-3

[40] KIM HJ, KIM SY, KIM DH, PARK JS, JEONG SH et al. Crosstalk between HSPA5 arginylation and sequential ubiquitination leads to AKT degradation through autophagy flux. Autophagy 2021; 17: 961–979. https://doi.org/10.1080/15548627.2020.1740529

[41]	GAO S, CHENG QC, HU YG, TAN ZZ, CHEN L et al. Ln-cRNA AK148321 alleviates neuroinflammation in LPS-stimulated BV2 microglial cell through regulating microRNA-1199-5p/HSPA5 axis. Life Sci 2021; 266: 118863. https://doi.org/10.1016/j.lfs.2020.118863

[42]	ELFIKY AA, BAGHDADY AM, ALI SA, AHMED MI. GRP78 targeting: Hitting two birds with a stone. Life Sci 2020; 260: 118317. https://doi.org/10.1016/j.lfs.2020.118317

[43]	SHEN LD, QI WH, BAI JJ, ZUO CY, BAI DL et al. Resibufogenin inhibited colorectal cancer cell growth and tumorigenesis through triggering ferroptosis and ROS production mediated by GPX4 inactivation. Anat Rec (Hoboken) 2021; 304: 313–322. https://doi.org/10.1002/ar.24378

[44]	ASPERTI M, BELLINI S, GRILLO E, GRYZIK M, CANTAMESSA L et al. H-ferritin suppression and pronounced mitochondrial respi ration make Hepatocellular Carcinoma cells sensitive to RSL3-induced ferroptosis. Free Radic Biol Med 2021; 169: 294–303. https://doi.org/10.1016/j.freeradbiomed.2021.04.024

[45]	SHAO Y, JIA H, HUANG L, LI S, WANG C et al. An Original Ferroptosis-Related Gene Signature Effectively Predicts the Prognosis and Clinical Status for Colorectal Cancer Patients. Front Oncol 2021; 11: 711776. https://doi.org/10.3389/fonc.2021.711776